Applied Catalysis B: Environmental 205 (2017) 327–339

Contents lists available at ScienceDirect

Applied Catalysis B: Environmental

journal homepage: www.elsevier.com/locate/apcatb

Modulating oxone-MnO_x/silica catalytic systems towards ibuprofen degradation: Insights into system effects, reaction kinetics and mechanisms

Jia-Cheng E. Yang[a,b], Baoling Yuan[c,*], Hao-Jie Cui[a], Shaobin Wang[d], Ming-Lai Fu[a,*]

[a] Key Laboratory of Urban Pollutant Conversion, Institute of Urban Environment (IUE), Chinese Academy of Sciences (CAS), No. 1799, Jimei Avenue, Xiamen 361021, China
[b] University of Chinese Academy of Sciences (UCAS), Beijing 100039, China
[c] College of Civil Engineering, Huaqiao University, Xiamen 361020, China
[d] Department of Chemical Engineering, Curtin University, GPO Box U1987, Perth, WA 6845, Australia

ARTICLE INFO

Article history:
Received 9 November 2016
Received in revised form 7 December 2016
Accepted 19 December 2016
Available online 21 December 2016

Keywords:
Oxone
Ibuprofen
MnO_x/silica
Humic acid
Inorganic ions

ABSTRACT

Heterogeneous processes activated persulfate for organic degradation is increasingly recognized as an environmentally important remediation technology. However, manipulating persulfate oxidation processes with desirable decontamination effectiveness is still underdeveloped. Towards this goal, we systematically investigated the catalytic behaviors of Oxone-MnO_x/silica systems towards aqueous ibuprofen (IBU) degradation in terms of system effects, reaction kinetics and mechanisms. MnO_x/SBA-15 (MS) demonstrated variable catalytic Oxone efficacies towards IBU removal at different solution pHs. Meanwhile, the catalyst supports and FeO_x co-doping within MS also produced significant impacts on catalytic Oxone efficacy. Moreover, the catalytic Oxone efficacies of MS for IBU degradation were generally inhibited by humic acid, NO_3^-, HCO_3^-, SO_4^{2-} and PO_4^{3-} to different extents at low/high levels. Interestingly, Cl^- at low concentrations (2 mM) obviously inhibited IBU removal by Oxone-MS, while Cl^- at high concentrations (20 mM) greatly enhanced IBU removal. Kinetic studies implied that IBU removal by Oxone-MnO_x/silica systems using two first-order kinetic models was closely related to the extents of the interferences of synthetic conditions and water chemistry components. The surface electron transfer between $\equiv MnO_x(OH)_y$ species of MS and HSO_5^- of Oxone was responsible for the formation of reactive oxygen radicals, thus contributing to IBU degradation. Liquid chromatography–mass spectrometry was employed to identify oxidation products of IBU, and reaction pathways of IBU oxidation were accordingly proposed.

1. Introduction

In the past decades, catalytically activated persulfate-based advanced oxidation processes (APS-AOPs) have been promising in oxidizing various contaminants [1–11]. Understanding the basic principles controlling the properties of materials for persulfate activation and addressing the technical bottlenecks of APS-AOP applications are keys to obtaining desirable decontamination effectiveness. Previous studies showed that the intrinsic properties of materials would control the catalytic behaviors of APS for contaminant oxidation/destruction via reactive oxygen radicals (RORs) [6,7,12–18]. Additionally, ROR generation/distribution was dependent on the acid-base property of target solutions [19,20]. Given this, one can hypothesize that catalysts with a certain characteristic or different properties under varied acid-based conditions for persulfate activation would lead to the changes of ROR-dependent oxidation/decontamination efficacies. Nevertheless, till now, the understanding on manipulating the catalytic systems of Oxone and supported-MnO_x composites under varied acid-base conditions for the removal of aqueous emerging contaminants like ibuprofen (IBU) is generally ambiguous.

On the other hand, water chemistry constituents will affect the efficacies of APS-AOP-based remediation implementations. Cl^- ions, as ubiquitous matrix in wastewaters, were reported to inhibit the degradation of azo dyes in low concentrations (<10 mM) but enhance the degradation in high concentrations (>100 mM) for Co^{2+}/Oxone system [21]. In a sonochemical Fe^0-catalyzed persul-

* Corresponding authors.
E-mail addresses: blyuan@hqu.edu.cn (B. Yuan), mlfu@iue.ac.cn, fuminglai@gmail.com (M.-L. Fu).

http://dx.doi.org/10.1016/j.apcatb.2016.12.046
0926-3373/

fate system, completely opposite observation was reported for sulfadiazine destruction [22]. Meanwhile, insignificant or completely inhibitory effects of Cl^- ions have also been revealed in some other APS systems for removal of organic chemicals [23,24]. Considering the foregoing cases, one can be sure that revealing the effects of water quality parameters is not straightforward in APS-AOPs due to the variations of water chemistry constituents, target contaminants and heterogeneous catalysts. However, such knowledge is still not conclusive, which hampers the manipulations of APS-AOPs and the development of efficacy/mechanism-based kinetic models for practical applications.

Developing environmental conditions-related kinetic models are vital in APS-AOPs towards pollutant clean-up processes. To date, most published work concerning detoxification applications of APS-AOPs mainly focused on the investigations into the removal/decontamination efficiency of pollutants using different activation/catalytic methods for persulfate by comparison. Few fragmentary studies have described the kinetics of contaminant removal by APS-AOPs [23,25,26]. Moreover, comparisons of different kinetic models based on the types of contaminants, the methods of PS activation or the environmental conditions are still not available. Thus, we provide such a comparison of two kinetic models for IBU removal by Oxone-MnO_x/silica systems under different conditions.

Interactions between PS and transition-metal oxides in aqueous phases had been widely explored in PS activation and RORs evolution. As suggested in literatures [13,17,27–31], radical and nonradical pathways are widely accepted two processes for pollutant degradation. However, it should be noted that the surface activation mechanisms of PS with activators/catalysts differ greatly under varied conditions. In an Oxone-$CuFe_2O_4$ system [28], Cu(II)-Cu(III)-Cu(II) redox process was responsible for ROR formation, while for Oxone activation using carbon catalysts [13,32], both radical and nonradical pathways were suggested contributing to organic degradation. Therefore, for a systematic research, the current work aims at ascertaining the interactions of Oxone and MnO_x/SBA-15 systems and the behaviors of resultant RORs towards IBU degradation. MnO_x/SBA-15 and IBU were employed in our work as a target activator and probe contaminant, respectively, because of (i) the high abundance, relatively low price and environmental friendliness of Mn/silica-based oxides [33] as well as the higher catalytic activities of supported MnO_x than bare MnO_x [18,34], and (ii) the frequent occurrence of IBU (an anti-biodegradation drug) in wastewaters with its aqueous concentration being up to ug/L levels and potential risks to the ecosystems [35,36]. The reaction pathways/mechanisms of Oxone-MnO_x/silica systems for IBU degradation could be well compared with reported ones in APS/non-APS based AOPs [37–42]. The current study will cast light on modulation of the catalytic behaviors of Oxone-MnO_x/silica systems towards ibuprofen IBU degradation, thus serving as a reference for designing versatile functional catalysts for specific environmental applications. Moreover, the pioneering work on reaction kinetics and mechanisms of IBU by Oxone-MS system will enrich our understanding on the ROR-induced pollutant degradation pertinent to system effects and reaction mechanisms.

2. Experimental section

2.1. Materials

All chemicals used herein are of analytical grade and used without further purification, and deionized water was used to prepare all solutions. A series of focused materials, i.e., ordered mesoporous silica (SBA-15), MnO_x/SBA-15 (MS_X(Y,Z)), MnO_x/kaolin (MK_X(Y,Z)), MnO_x/diatomite (MD_X(Y,Z)), FeO_x/SBA-15(FS_X(Y,Z)) and FeO_x-MnO_x/SBA-15(FMS_X(Y,Z)) were synthesized based on previous protocols [18,43]. X, Y and Z stand for the weight rates of Mn/supporter (wt%), calcination temperature (K) and time (h), respectively, and more information on materials synthesis can be found in Table S1 (Supplementary materials, SM).

2.2. Characterizations

X-ray diffraction (XRD) spectra of samples were recorded on an X′Pert PRO diffractometer (PANalytical, Holland, Cu K_α, λ = 0.15406 nm) with 40 kV accelerating voltage and 40 mA current. The scanning electron microscopy (SEM) images (Figs. S6–S12) and energy dispersive X-ray (EDX) spectra (Figs. S13 and S14) of samples were obtained by an S-4800 (Hitachi, Japan), and the transmission electron microscopy (TEM) (Fig. S6) images of powder samples were determined on an S-7650 equipment (Hitachi, Japan). N_2-adsorption/desorption isotherms and pore structures of samples were measured by an ASAP 2020M + C apparatus (Micromeritics, USA) at 77 K (Fig. S15). The surface elemental information of fresh and used samples was characterized by X-ray photoelectron spectroscopy (XPS) operated on a Kratos Amicus spectrometer (Shimadzu, Japan) equipped with Mg K_α X-ray source. The zeta potentials of samples were determined using a Zeta-PALS analyzer (Malvern, United Kingdom) for points of zero charge (pH_{PZC}). Prior to zeta-potential tests, all aqueous samples (~3 g/L) with varied pH values were equilibrated for at least 24 h. Electron paramagnetic resonance (EPR) measurements were performed using a Bruker EMX-2.0/2.7 EPR spectrometer with dual cavities, X-band, 100 kHz, and microwave frequency, 9.53 GHz. The spectra were obtained at room temperature. More details on physicochemical characteristics of materials can be found in SM.

2.3. Batch experiments

Batch degradation experiments, unless otherwise specified, were conducted in 100-mL flat conical flasks with ground-in glass stoppers, containing 80 mL IBU solutions. Diluted HNO_3 and NaOH solutions were used to adjust the initial pHs of target samples, and the pH values of the solutions were measured before and after reaction. Degradation experiments were initiated upon introducing both MnO_x-based composites and Oxone into the glass flasks simultaneously. At predetermined intervals, IBU samples (2 mL) were taken and quickly quenched with 0.5 mL methanol, followed by filtering using 0.45 μm cellulose acetate membranes for residue analysis. All the experiments were carried out in duplicate or triplicate in a rotary vibrator at 300 rpm/min under aerobic conditions (298 ± 2 K). In addition, control experiments were also performed. The residual concentrations of IBU in solutions were analyzed using a high performance liquid chromatography (HPLC) (Agilent 1260, USA) system with a mobile phase of 70/30 (v/v) acetonitrile-phosphate buffer solution (20 mM, pH 2.1) at a flow rate of 1 mL/min and 303 K. The intermediates were measured by HPLC/mass spectrometry (MS) (Agilent 1100, USA) (see SM for details). The aqueous concentrations of Mn ions were measured by inductively coupled plasma mass spectrometry (ICP-MS) (Agilent 7500cx, USA). All data were reported in an average value with 95% of confidence level.

3. Results and discussion

3.1. System effects

3.1.1. Roles of synthetic conditions

The insignificant changes of background solution concentrations in the absence of Oxone and solid materials indicated that IBU was stable in solutions over the whole reaction, and IBU removal

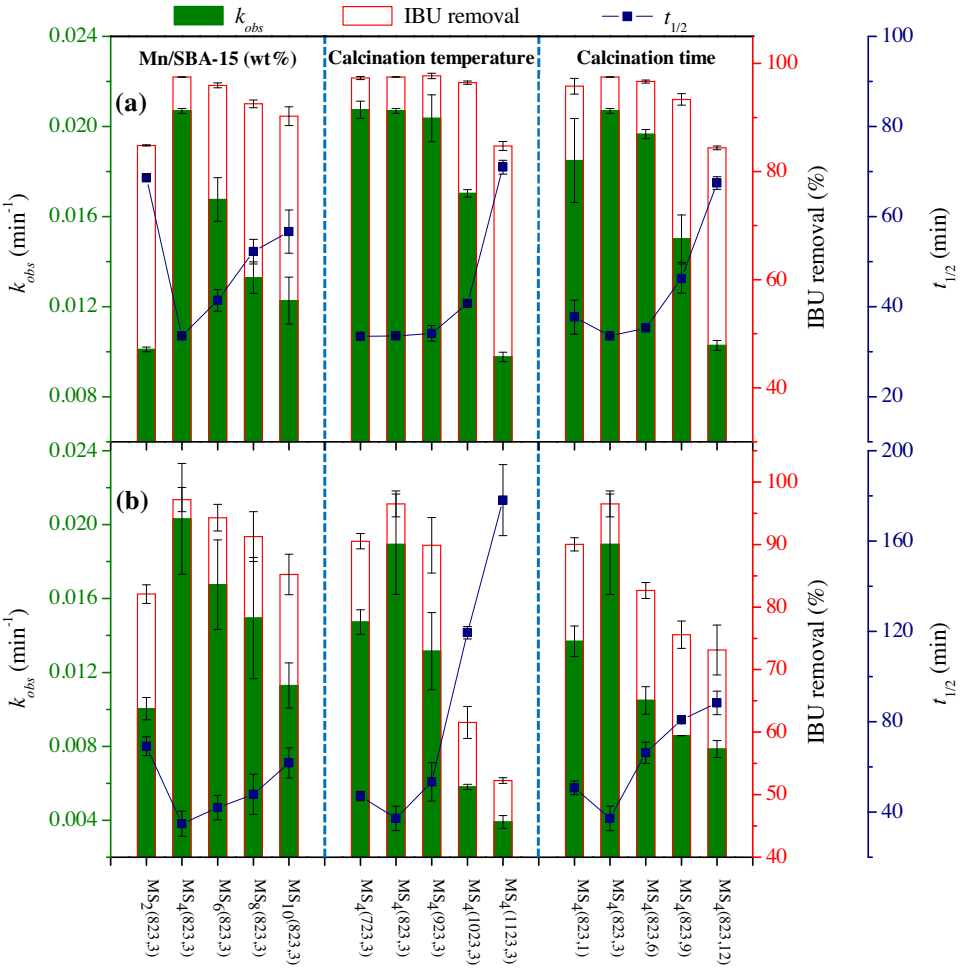

Fig. 1. Different MS catalysts-activated Oxone efficacy towards IBU oxidation degradation (k_{obs}, removal efficiency and $t_{1/2}$) under initial solution pHs 6.35 (a) and 10.00 (b) in aerobic environment. Other conditions: $[MS]_0$ = 1.0 g/L, $[IBU]_0$ = 24.24 μM, $[Oxone]_0$ = 6.25 mM, volume of 80 mL, temperature of 298 ± 2 K, and reaction time of 175 min. The error bars in symbols, unless otherwise mentioned, represent the ranges of multiple measurements (P < 0.05).

Table 1
Specific surface area, pore size and pore volume of SBA-15, diatomite, kaolin, MS_X(Y,Z), FS_X(823,3), MFS_X(823,3), MD_X(823,3) and MK_X(823,3) composites.

Samples	BET surface area (m^2/g)	Pore size (nm)	Pore volume (cm^3/g)	Samples	BET surface area (m^2/g)	Pore size (nm)	Pore volume (cm^3/g)
SBA-15	702.8096	5.4405	1.0197	FS_2(823,3)	528.9449	4.8371	0.6050
MS_2(823,3)	475.0256	6.5192	0.8029	FS_4(823,3)	500.0110	5.4140	0.6658
MS_4(823,3)	457.8572	6.3294	0.7634	FS_8(823,3)	494.9202	4.4904	0.5103
MS_6(823,3)	448.5817	6.3628	0.7538	MFS_6(823,3)	450.4608	5.0650	0.5589
MS_8(823,3)	416.5025	6.6503	0.7289	MFS_8(823,3)	447.3243	5.2504	0.5723
MS_{10}(823,3)	409.4191	6.5933	0.7101	MFS_{12}(823,3)	428.2300	4.9675	0.5142
MS_4(723,3)	429.4157	7.2133	0.7956	Diatomite	8.4529	10.8915	0.0282
MS_4(923,3)	449.0090	6.9078	0.7733	MD_2(823,3)	9.8099	10.3564	0.0307
MS_4(1023,3)	430.3947	6.9033	0.7657	MD_4(823,3)	11.4018	11.1729	0.0375
MS_4(1123,3)	414.9115	6.6712	0.7142	MD_8(823,3)	15.4427	10.8295	0.0516
MS_4(823,1)	456.6020	7.0358	0.8085	Kaolin	6.8656	11.0031	0.0239
MS_4(823,6)	457.2587	7.0407	0.8090	MK_2(823,3)	6.7895	12.4568	0.0255
MS_4(823,9)	456.3319	7.1414	0.8212	MK_4(823,3)	8.7063	12.1823	0.0334
MS_4(823,12)	437.1382	7.0718	0.7808	MK_8(823,3)	8.7206	13.6298	0.0373

by adsorption can be excluded (cf. Fig. S1). IBU removal (<17.5%) by supporters-activated Oxone oxidation was mainly due to the role of sole-Oxone oxidation, which ruled out the roles of supporters in Oxone activation (Fig. S1(b)). Note that IBU removal (~12%) by sole-Oxone oxidation is limited in the current study. However, upon Oxone and MnO_x-based catalysts simultaneously adding into IBU solutions, significant degradation occurred (Figs. 1 and 3 and S2–S4), implying that Oxone activation by MnO_x-based materials was the main process for IBU degradation. Fig. 1 shows that, in general, IBU removal efficiencies under initial solution pH values of 6.35 and 10.00 firstly increased and then decreased with increased Mn weight loadings (wt%), calcination temperature and time, indicating a distinct dependence of IBU degradation by Oxone-MS systems on the synthetic conditions of MS catalysts. This is similar to our previous report on butyl paraben removal [18]. The variations of IBU degradation under solution pH 10.00 are more remarkable than those of solution pH 6.35 (see details in Figs. 1, S2 and S3). However, the pseudo first-order reaction constants of IBU degra-

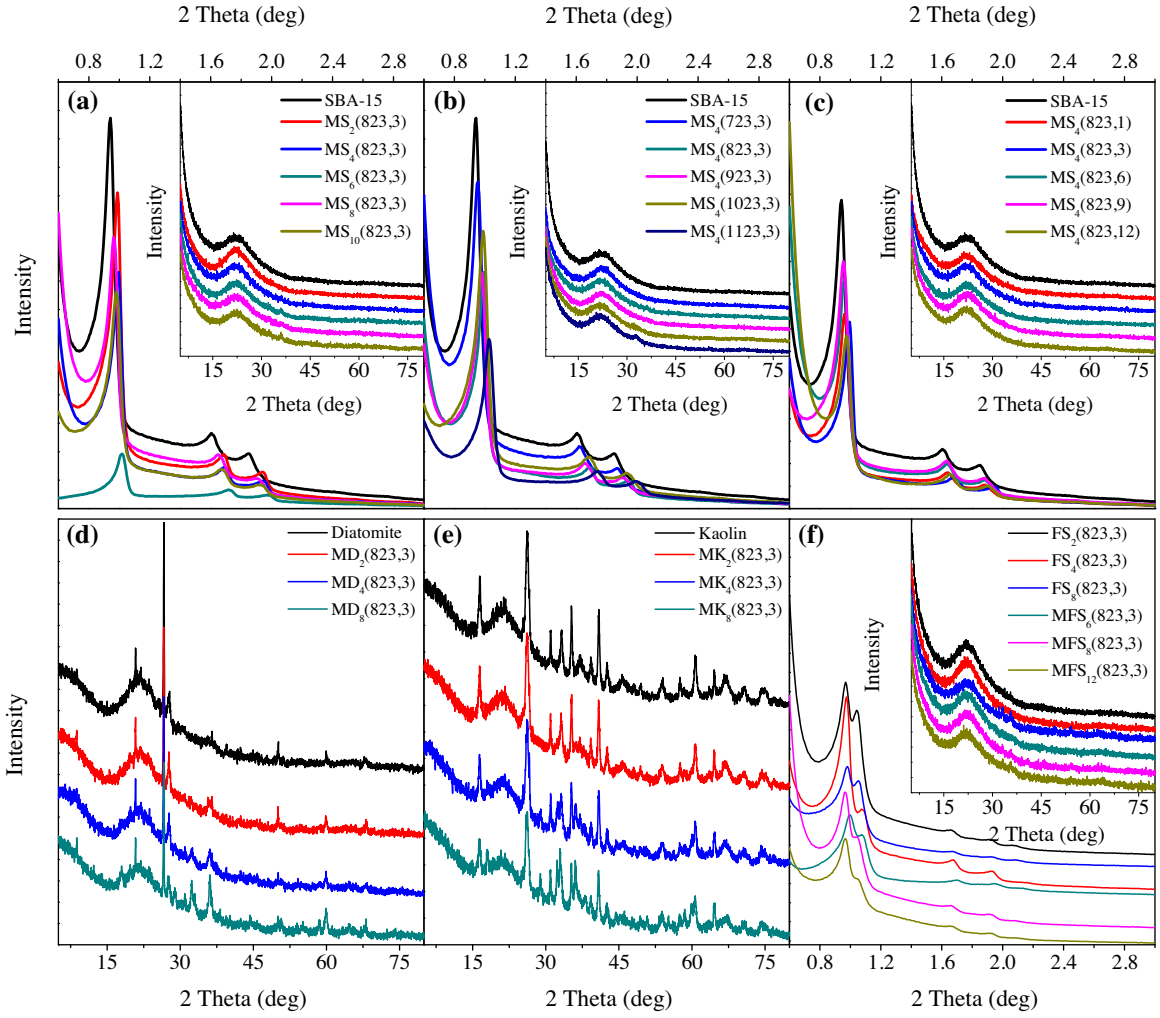

Fig. 2. XRD patterns of SBA-15 and $MS_X(Y,Z)$ with different Mn/SBA-15 wt ratios (a), calcination temperatures (b) and hours (c), diatomite and $MD_X(823,3)$ (d), kaolin and $MK_X(823,3)$ (e), and $FS_X(823,3)$ and $MFS_X(823,3)$ (f).

dation at solution pH 6.35 are generally higher than those obtained at solution pH 10.00 (Table S2). These results suggest that synthetic conditions of MS composites demonstrated varied roles in regulating catalytic Oxone efficacies for organic pollutant degradation under changed solution pHs. The changes in XRD patterns, BET surface areas, pore features, pH_{PZC} and SEM images of MS with increased Mn/SBA-15 wt ratios (see Figs. Fig. 2(a), S6 and S7, Table 1, and Ref. [13]) implied that the crystal phases, specific surface area, pore characteristics, surface charge and morphology of $MS_X(823,3)$ played insignificant roles in Oxone activation. The effects of the changes in surface morphologies and crystal phases of $MS_4(Y,3)$ and $MS_4(823,Z)$ on catalytic Oxone performance can be excluded (refer to Figs. 2 (b,c), S8 and S9). Interestingly, a similarly consistent trend was observed among the changes in IBU removal and the variations of BET surface area with calcinations temperature and time of MS increased (Fig. 1 and Table 1). Yet, the pore characteristics of $MS_4(Y,3)$ and $MS_4(823,Z)$ may be not the main factor controlling Oxone activation. If that were true, the changes in IBU removal by $MS_4(Y,3)$/$MS_4(823,Z)$-Oxone systems under solution pH 10 should be not so obvious. But that is not the case. Additionally, the effects of the release of Mn ions are also ruled out due to their limited Oxone activation performance at concentration of 40 mg/L (Fig. S1(b)) and their low release concentrations (far less than 1 mg/L). Previous work found that the changes of Mn/SBA-15 wt ratios, calcinations temperature and time could control the changes of Mn oxidation states [44], and that the changes of supported MnO_x species in Mn valences could regulate the formation and distribution of RORs in Oxone-MS systems [18]. Meanwhile, solution pHs will induce effects on Oxone efficacy towards organic degradation via changing the types of RORs like $SO_4^{\bullet-}$ and $^{\bullet}OH$ [20]. So, the differences in catalytic Oxone performance for different MS materials under varied solution pHs are likely to be the combined effects of the polytropical Mn oxidation states of MS and the varied solution pHs.

It is evident that the supports and promoter like FeO_x in MS produced different effects on catalytic Oxone activation (Figs. 3 and S4). For MK, increasing Mn weight loadings led to a decreased catalytic Oxone activation, while for MD, the catalytic Oxone performance first experienced a slight increase and then an obvious decrease in terms of IBU removal (i.e., removal efficiency, k_{obs} and $t_{1/2}$) (Figs. 3 and S4, Table S2). Insignificant variations on SEM images of MK and MD were observed compared to the bare supports (Figs. S10 and S11), which ruled out the effects of microscopic morphologies on Oxone activation performance. The inconsistency of the changes between BET surface areas/XRD patterns and IBU removal for MK and MD (Fig. 2(d,e) and Table 1) indicated the negligible impacts of their pore features and crystal phases on catalytic Oxone efficacy. Therefore, the changes in the MnO_x species and Mn oxidation states on/within the different supports are likely the main factors in regulating catalytic Oxone efficacy [44–46]. The differences of MK, MD

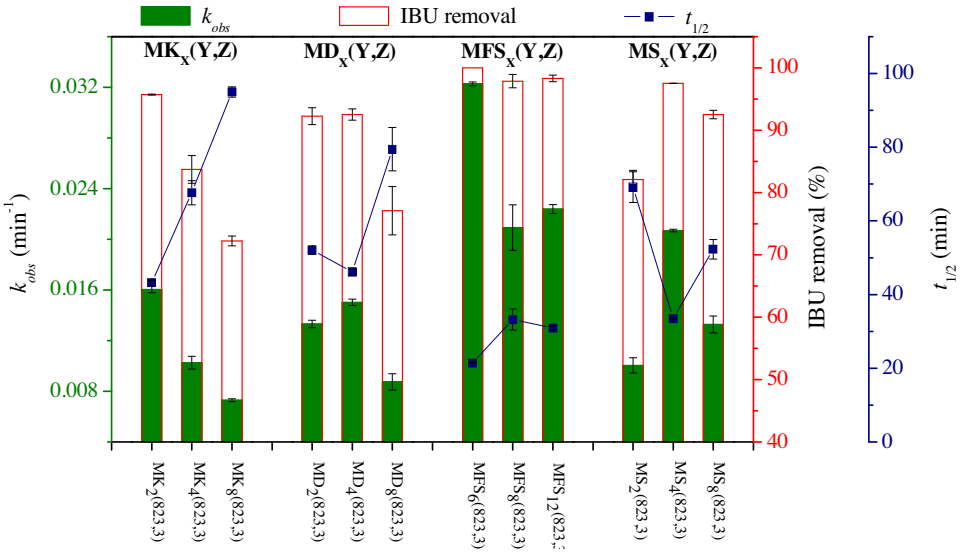

Fig. 3. Comparison on IBU oxidation degradation (k_{obs}, removal efficiency and $t_{1/2}$) by MK, MD MFS and MS activated Oxone under initial solution pH 6.35 in aerobic environment. Other conditions: $[MK]_0 = [MD]_0 = [MFS]_0 = [MS]_0 = 1.0$ g/L, $[IBU]_0 = 24.24$ μM, $[Oxone]_0 = 6.25$ mM, volume of 80 mL, temperature of 298 ± 2 K, and reaction time of 175 min.

and MS in IBU removal (Fig. 3) suggest that the supporters played vital roles in modulating catalytic Oxone efficacy probably by regulating the formation of MnO_x species within supporters [14,16,47]. The effects of activating species on catalytic Oxone efficacy are also studied by comparing IBU removal by FS-Oxone, MS-Oxone and FMS-Oxone systems. It is clear that IBU removal by FS-Oxone (Fig. S5) is very low (around 15%, much lower than that of MS) if that of by sole-Oxone were excluded. This can probably be ascribed to the higher catalytic Oxone properties of MnO_x than those of FeO_x despite of its excellent catalytic ability for H_2O_2 decomposition into •OH [2,48]. Unexpectedly, FeO_x co-doping within MS composites (i.e., MFS) greatly enhanced their catalytic Oxone abilities; however, the over-doping of FeO_x in FMS resulted in a slightly decreased IBU removal – but still higher than that by MS (cf. Figs. 3 and S4(c,d), Table S2). This suggests a dual effect of co-doping of FeO_x on catalytic Oxone performance of FMS. Analysis on XRD, SEM and surface area characterizations suggests an unimportant role of the pore characteristics, surface morphology characteristics and crystal phases of FS and MFS in manipulating catalytic Oxone performance (Figs. 2 (f) and S12, Table 1) Based on previous work [49], FeO_x co-doping could regulate the formation of activating species (mainly MnO_x) and accelerate the electron transfer in solid/water interface for FMS-Oxone systems, thus contributing to the enhanced IBU removal. The notable decline in k_{obs} might be due to the decreased active sites of activating species caused by excessive co-doping of FeO_x. More evidence should be explored on this issue in future work.

Taking the characterizations of XRD, SEM and N_2 adsorption/desorption isotherms, IBU removal and previous work into account, the crystal phases, surface morphologies characteristics, pore sizes and surface areas are not the main factors for regulating catalytic Oxone performance of the supported MnO_x composites, and the nature of activating species is recognized as the possible elements responsible for Oxone activation [16,47,50,51]. Above all, the varied roles of synthetic conditions may occur commonly among heterogeneous catalysts for PS activation. If the roles could not been fully taken into account for designing functional materials for environmental applications, the removal of target contaminants would be over- or under-estimated, which may cause a partial/erroneous understanding and prediction on the catalytic properties of materials. Therefore, more evidences for revealing these roles are highly needed in future work.

3.1.2. Influences of solution chemistry

3.1.2.1. Solution pHs. Considering the above results and the homogeneity of SBA-15, $MS_4(823,3)$ was selected as a model catalyst for Oxone activation to elucidate the influences of solution chemistry. It is clear that $MS_4(823,3)$ demonstrated a robust and steady catalytic Oxone activation for IBU degradation at a wide range of initial solution pHs from 2.81 to 10.00; however, a significant decline in IBU degradation occurred when the initial solution pH further increased to 11.40 (Fig. 4(a) and Table S3). The removal efficiencies of IBU by Oxone alone in the absence of $MS_4(823,3)$ under different initial solution pHs were less than 15%, confirming that interacting of Oxone with $MS_4(823,3)$ to form RORs was the key driving-force governing IBU degradation. In the current study, solution pH played, at least, three key roles in Oxone-$MS_4(823,3)$ systems for IBU degradation. First, solution pH can change the surface charge of $MS_4(823,3)$. The pH_{PZC} of $MS_4(823,3)$ was determined to be 2.25. When $MS_4(823,3)$ was dispersed in solutions with pH of <2.25, its surface was positively charged, conversely, negatively charged. Second, solution pH can govern the distribution of Oxone-based species. The pK_{a1} and pK_{a2} of H_2SO_5 are 0 and 9.4, respectively [20]. Therefore, it is quite clear that HSO_5^- was the main Oxone species at pH ranging from 2.81 to 9.4, while, at pH > 9.4, the proportion of SO_5^{2-} would greatly increase. Third, solution pH can influence the fraction of IBU species. If the solution pHs were below the pK_a of IBU (3.5–4.9 [52]), IBU were principally supposed to be in the molecular form or positively charged, while above pK_a, anionic IBP molecules were the predominant species. Moreover, the difference in the calculated pHs after reactions and the measured solution pHs before and after reactions indicated that Oxone would have particular ability to buffer the solution pH via the released H^+ ions from its decomposition (see Table S3 and reaction 1). When Oxone (6.25 mM) was added to solutions with initial pH values of 2.81–10.00, the solution pHs would be reduced to 2.32–2.50, which were close to the pH_{PZC} of $MS_4(823,3)$ and far less than the pK_{a2} of H_2SO_5, thereby promoting the interactions between HSO_5^- and electrically neutral $MS_4(823,3)$ via hydrogen bonds to form RORs and the degradation reactions occurred between negatively charged RORs (like $SO_4^{\bullet-}$) and positively charged IBU molecules.

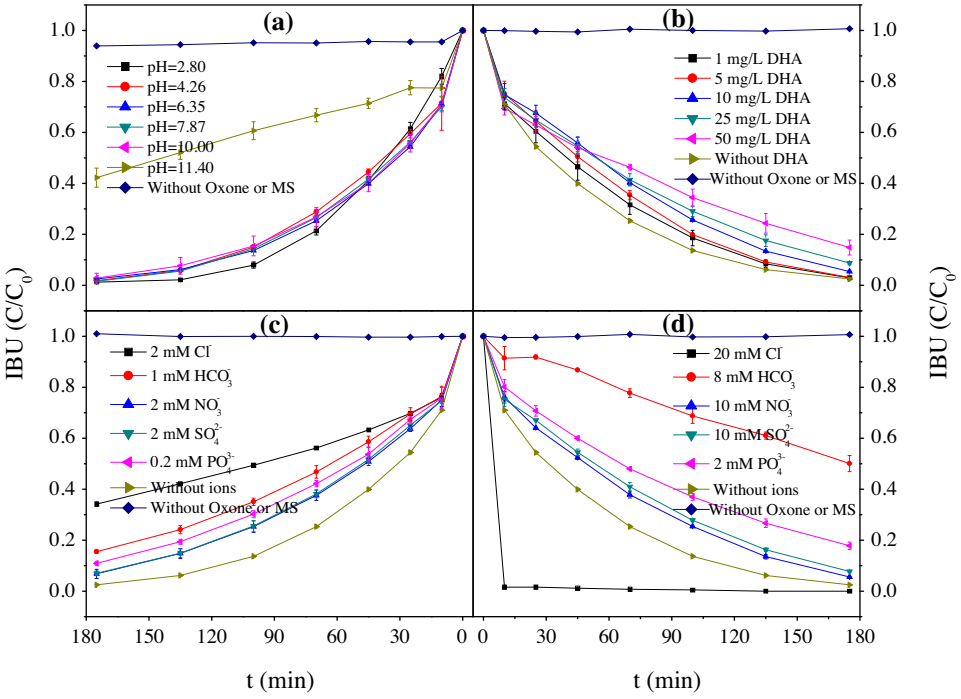

Fig. 4. IBU oxidation degradation by Oxone-MS_4(823,3) system under different solution chemistry in aerobic environment. Other conditions: $[Oxone]_0$ = 6.25 mM, $[MS_4(823,3)]_0$ = 1.0 g/L, pH_0 = 6.35 ± 0.2 (for (b–d)), volume of 80 mL, temperature of 298 ± 2 K, and reaction time of 175 min.

However, when initial solution pH increased to 11.40, the buffering efficacy of Oxone was largely reduced (evidenced by the pH_{after} value of 3.02, Table S3), which inhibited Oxone activation due to electrostatic repulsions between MS_4(823,3) and Oxone species and thus influenced the ROR formation. This finding is analogous to our previous report [11]. Note that MS_4(823,3) itself possesses no buffering ability against solution pH changes. Thus, considering the aforementioned processes, it can be understood that the effects of initial solution pHs on catalytic Oxone efficacies is a trade-off of the cross-effects of electrostatic reactions between Oxone species and catalysts as well as target pollutants. In addition, the impacts of Mn ions released from MS_4(823,3) on IBU removal were proved to be limited considering their low concentrations under varied pHs (far less than 1 mg/L) (see Fig. S1(b)).

$$KHSO_5{\cdot}1/2KHSO_4{\cdot}1/2\,K_2SO_4 \rightarrow 2\,K^+ + HSO_5^- + 1/2H^+ + SO_4^{2-} \quad (1)$$

3.1.2.2. Dissolved humic acid (DHA). Nature organic matter (NOM) is commonly found in water bodies. Specific moieties like phenols and amines in NOM can directly react with RORs and can also compete with organic pollutants with RORs, thus impairing the eliminations of target contaminants. For this purpose, we used commercially accessible humic acid (Sigma-Aldrich) as a NOM surrogate. As presented in Fig. 4(b), DHA in Oxone-MS_4(823,3) systems has retarded IBU removal, and the k_{obs} of IBU decreased linearly with increased DHA concentrations (Table S3). However, it is found that the extent of the decrease in k_{obs} (by 46.82%) was 3.7 times larger than that of IBU removal efficiency (by 12.64%) when the concentrations of DHA increased from 0 to 50 mg/L (Table S3). It was reported that the reaction rate constants of humic acid with $SO_4^{\bullet-}$ and •OH were $(5.1 \pm 0.5) \times 10^3$ $(mg\text{-}C/L)^{-1}\,s^{-1}$ and $(2.5 \pm 0.4) \times 10^4$ $(mg\text{-}C/L)^{-1}\,s^{-1}$, respectively [53]. So, a reasonable explanation for such phenomenon might be the quenching roles of DHA via its competing effect, despite the fact increasing DHA concentrations reduced solution pHs because of its presence of –COOH groups (Table S3). Note that the presence of DHA in Oxone-MS_4(823,3) systems did not cause significant effects on the reaction kinetics of IBU degradation, which was confirmed by the fitting results using the first-order kinetic model (Table S3).

3.1.2.3. Inorganic anions. Fig. 4(c,d) depicts the effects of inorganic anions with low and high levels on IBU removal by MS_4(823,3) activated Oxone. It is evident that the roles played by different anions differed greatly. For example, the presence of 2 mM Cl^- resulted in an inhibition on the catalytic Oxone efficacy of MS_4(823,3) (decreased by 67.48% in k_{obs}), while the catalytic Oxone efficacy was largely enhanced by 20 mM Cl^- (increased more than 20 times in k_{obs}), suggesting a concentration-based dual effect of Cl^- on IBU removal. It is widely accepted that Oxone species and their derived RORs in the presence of Cl^- can induce the formation of active chloride species (like Cl_2, Cl• and HOCl) via either radical-based pathways or non-radical pathways (cf. reactions (2) – (10)) [24,54,55]. So, in the current system, the decreased IBU removal at low Cl^- concentration probably resulted from the reduced amount of $SO_4^{\bullet-}$ and •OH and the formation of less reactive chlorine species like Cl• and HOCl via direct or radical-based chain reactions of Cl^-; while the enhanced IBU removal was likely due to the formation of highly reactive Cl_2 with a large amount. The presence of Cl^- has changed the whole reaction kinetics of target organic pollutant via regulating the formation and distribution of active radicals. The curves of IBU removal in the presence of Cl^- (shown in Fig. 4(c,d), Table S3) verified such conclusion. Note that the dual effects of Cl^- ions (i.e., accelerating and inhibitory effect) on degradation of organic pollutants by APS-AOPs varied considerably because of the difference of organic pollutants and PS-based oxidation systems [21,22,55]. Besides the fact that the resultant chloride species can change the removal efficiency and reaction kinetics of IBU by Oxone-MS_4(823,3) system, chloride species can also induce the formation of some chlorinated by-products, which may inhibit IBU

mineralization and may also increase the toxicity of IBU byproducts [55].

$$Cl^- + HSO_5^- \rightarrow SO_4^{2-} + HOCl \quad (2)$$

$$2Cl^- + HSO_5^- + H^+ \rightarrow SO_4^{2-} + H_2O + Cl_2 \quad (3)$$

$$SO_4^{\bullet-} + Cl^- \leftrightarrow SO_4^{2-} + Cl, k_{4f} = 3.2 \times 10^8\ M^{-1}\ S^{-1}; k_{4r} = 2.1 \times 10^8\ M^{-1}\ S^{-1} \quad (4)$$

$$Cl + Cl^- \leftrightarrow Cl_2^{\bullet-}, k_{5f} = 7.8 \times 10^9\ M^{-1}\ S^{-1}; k_{5r} = 5.7 \times 10^4\ S^{-1} \quad (5)$$

$$2Cl_2^{\bullet-} \rightarrow Cl_2 + 2Cl^-, k_6 = 2.1 \times 10^9\ M^{-1}\ S^{-1} \quad (6)$$

$$Cl_2^{\bullet-} + H_2O \rightarrow HOCl^{\bullet-} + Cl^- + H^+, k_7 < 10^2\ S^{-1} \quad (7)$$

$$OH + Cl^- \leftrightarrow HOCl^{\bullet-}, k_{8f} = 4.3 \times 10^9\ M^{-1}\ S^{-1}; k_{8r} = 6.1 \times 10^9\ M^{-1}\ S^{-1} \quad (8)$$

$$HOCl^{\bullet-} + H^+ \leftrightarrow Cl + H_2O k_{9f} = 2.6 \times 10^{10}\ M^{-1}\ S^{-1}; k_{9r} = 1.6 \times 10^5\ S^{-1} \quad (9)$$

$$HOCl^{\bullet-} \leftrightarrow Cl + OH k_{10f} = 6.1 \times 10^9\ S^{-1}; k_{10r} = 4.3 \times 10^9\ M^{-1}\ S^{-1} \quad (10)$$

It can be seen that IBU removal by bicarbonate-containing Oxone-MS_4(823,3) systems experienced an obvious loss compared to that without HCO_3^-, and the extent of the decrease in IBU removal was positively correlated to the HCO_3^- concentrations (Fig. 4(c,d), Tables 3 and S3). To fully understand HCO_3^- impacts, pH changes and reaction kinetics were measured. In general, the buffering ability of HCO_3^- increased with its increased concentrations, confirmed by the higher pH values after reaction, while IBU removal in the presence of HCO_3^- can still be well fitted by the first-order kinetics in spite of low removal efficiencies (see Table 2). Accordingly, three possible reasons are given to explain such findings: one is that HCO_3^- as a buffering/metal complexing agent had changed MS_4(823,3) surface properties, thus weakening its catalytic ability for Oxone activation and reducing the formation of reactive radicals like $SO_4^{\bullet-}$ and OH for IBU degradation [24]; the other is that HCO_3^- as a scavenging agent induced the formation of $HCO_3^{\bullet-}$ via reactions (11) and (12), and the resultant $HCO_3^{\bullet-}$ showed low reaction activity towards IBU [22]. The last is the result of greater inhibiting effect of HCO_3^- at 8 mM, because the higher concentration of HCO_3^- (like 8 mM) could maintain high solution pH levels over the reaction (see Table 3). At high pH levels, the negatively charged MS_4(823,3) could repel the approach of negative HSO_5^- and anionic IBU. In view of observed multiple effects of $HCO_3^{\bullet-}$ on organic degradation in APS-based oxidation systems [22,24,56,57], in-depth investigations are anticipated.

$$SO_4^{\bullet-} + HCO_3^- \rightarrow SO_4^{2-} + HCO_3, k_{11} = 9.1 \times 10^6\ M^{-1}\ S^{-1} \quad (11)$$

$$OH + HCO_3^- \rightarrow OH^- + HCO_3, k_{12} = 8.5 \times 10^8\ M^{-1}\ S^{-1} \quad (12)$$

$$SO_4^{\bullet-} + NO_3^- \rightarrow SO_4^{2-} + NO_3, k_{13} = 5.5 \times 10^5\ M^{-1}\ S^{-1} \quad (13)$$

$$OH + NO_3^- \rightarrow OH^- + NO_3, k_{14} < 5 \times 10^5\ M^{-1}\ S^{-1} \quad (14)$$

$$SO_4^{\bullet-} + PO_4^{3-} \rightarrow SO_4^{2-} + PO_4^{\bullet2-} \quad (15)$$

$$OH + PO_4^{3-} \rightarrow OH^- + PO_4^{\bullet2-} \quad (16)$$

NO_3^- and SO_4^{2-} as common anions in wastewaters were found to exert slight inhibition to IBU degradation at their low and high concentrations. For NO_3^-, the inhibition might be a result of the scavenging reactions between NO_3^- and $SO_4^{\bullet-}$/•OH [22] (reactions (13) and (14)) and the subsequent formation of nitrate radicals ($NO_3^{\bullet}$) of less reactivity, which thereof reduced IBU removal. The adverse effects of SO_4^{2-} was likely due to the reduced half-reaction reduction potential of $SO_4^{\bullet-}/SO_4^{2-}$ – which was largely related to the concentration of SO_4^{2-} [58], thus affecting Oxone activation to form RORs for IBU degradation. It is clear that the addition of phosphate ions (PO_4^{3-}) resulted in decreased IBU removal by Oxone-MS_4(823,3) (Fig. 4(c,d)), which agreed with a previous report [22]. Increasing the concentrations of PO_4^{3-}increased the inhibition effect, which can be verified by decreased IBU removal efficiencies or k_{obs} (Table S3). The negative effects exerted by PO_4^{3-}could be ascribed to two aspects: PO_4^{3-}as a quenching agent would react with $SO_4^{\bullet-}$/•OH with formation of less reactive $PO_4^{\bullet2-}$ (reactions (15) and (16)) [59,60] and PO_4^{3-}could partially complex with surface MnO_x species in MS_4(823,3) [22]. Additionally, Fig. 5(c) and Tables Table 3 and S3 also present the effects of organic scavengers, Oxone concentrations and MS_4(823,3) dosages, and solution temperatures. It should be noted that the effects of solution chemistry on performance of APS-AOPs for organic chemical destruction largely rely on the catalysts and pollutants coupling with the water chemistry constituents [20,61,62]. Therefore, a comprehensive evaluation on the impacts of solution chemistry is a necessity and will be conducive to develop models to trace the efficacy of APS-AOPs for organic clean-up.

3.2. Reaction kinetics

IBU degradation processes by MnO_x/silica activated Oxone under different conditions were fitted using the following two kinetic models:

$$\ln(C_t/C_0) = -k_{obs} \times t \text{(a)}$$

$$C_t = C_u + (C_0 - C_u) \times \exp(-k_p \times t) \text{(b)}$$

where C_t is the IBU concentration (μM) in solution at reaction time of t (min); C_0 represents the initial concentration of IBU (μM); k_{obs} and k_p denote the reaction constants of pseudo first order kinetic model and two-parameter pseudo-first-order kinetic model, respectively; and C_u stands for the residual concentration of nonreactive IBU (μM) in solution at infinite time.

The parameters (like k_{obs}, k_p and C_u) by model fitting with the above two models are listed in Tables 2 and 3, S2 and S3. Regardless of types of MnO_x-based materials, in general, IBU degradation by activated Oxone under acidic conditions can be better described by pseudo first order kinetic model than that under basic conditions (cf. Table S2), probably resulted from the difference of RORs in acidic and alkaline conditions. In Oxone-MS system, the presence of relatively complex water chemistry constituents/scavengers could also exert negative influences on IBU degradation, thus limiting the applicability of pseudo-first-order kinetic model (see equation (a)) for describing the catalytic Oxone performance and thereof decreasing the efficiency of manipulating/monitoring Oxone-based decontamination processes. On one hand, unfavorable impacts of Cl^- ions at low concentrations on IBU degradation in terms of removal efficiency and reaction kinetics confirmed such conclusion (Fig. 4(c,d), Table S3); on the other side, low correlation coefficients of R^2 for the cases of methanol and TBA suggested the detrimental effects on kinetic processes for IBU degradation (Fig. 5(c) and Table

Table 2
Fitted data for IBU degradation by active Oxone with different MnO_x-based materials using a two-parameter pseudo-first-order kinetics model (refer to Figs. 1 and 2 for more details on reaction conditions) †.

Materials	$pH_{initial}$	pH_{after}	k_p/min^{-1}	IBU removal/%	R^2	C_u/mM
MS_2(823,3)	6.35 ± 0.19	2.50 ± 0.06	9.72E−03 ± 4.81E-04	84.84 ± 0.11	0.9852 ± 0.0010	3.35E−02 ± 4.73E-02
MS_4(823,3)	6.35 ± 0.19	2.42 ± 0.04	2.38E−02 ± 6.36E-05	97.51 ± 0.00	0.9841 ± 0.0002	8.36E−01 ± 3.02E-02
MS_6(823,3)	6.35 ± 0.19	2.48 ± 0.02	1.58E−02 ± 2.52E-03	95.95 ± 0.47	0.9868 ± 0.0024	2.18E−01 ± 3.08E-01
MS_8(823,3)	6.35 ± 0.19	2.45 ± 0.04	1.20E−02 ± 1.12E-03	92.53 ± 0.71	0.9791 ± 0.0049	1.25E−14 ± 1.66E-14
MS_{10}(823,3)	6.35 ± 0.19	2.43 ± 0.03	1.20E−02 ± 1.70E-03	90.24 ± 1.74	0.9817 ± 0.0023	2.48E−01 ± 3.51E-01
MS_4(723,3)	6.35 ± 0.19	2.50 ± 0.04	3.09E−02 ± 5.98E-03	97.31 ± 0.28	0.9719 ± 0.0112	1.60E + 00 ± 6.58E-01
MS_4(923,3)	6.35 ± 0.19	2.49 ± 0.03	1.92E−02 ± 1.44E-03	97.70 ± 0.50	0.9869 ± 0.0078	2.38E−01 ± 3.37E-01
MS_4(1023,3)	6.35 ± 0.19	2.51 ± 0.04	1.46E−02 ± 1.11E-03	96.44 ± 0.29	0.9826 ± 0.0004	1.41E−13 ± 1.88E-13
MS_4(1123,3)	6.35 ± 0.19	2.51 ± 0.04	9.01E−03 ± 4.24E-05	84.72 ± 0.82	0.9769 ± 0.0068	7.60E−15 ± 9.80E-15
MS_4(823,1)	6.35 ± 0.19	2.53 ± 0.04	2.85E−02 ± 5.37E-04	95.79 ± 1.45	0.9666 ± 0.0063	2.05E + 00 ± 6.17E-01
MS_4(823,6)	6.35 ± 0.19	2.52 ± 0.06	3.56E−02 ± 1.22E-02	96.65 ± 0.28	0.9513 ± 0.0360	2.18E + 00 ± 1.01E + 00
MS_4(823,9)	6.35 ± 0.19	2.54 ± 0.05	1.90E−02 ± 1.48E-03	93.34 ± 1.07	0.9706 ± 0.0193	1.75E + 00 ± 1.00E + 00
MS_4(823,12)	6.35 ± 0.19	2.53 ± 0.05	1.37E−02 ± 4.13E-03	84.39 ± 0.33	0.9449 ± 0.0338	2.46E + 00 ± 2.19E + 00
MS_2(823,3)	10.00 ± 0.08	2.57 ± 0.15	1.66E−02 ± 2.07E-03	82.07 ± 1.49	0.9617 ± 0.0073	4.20E + 00 ± 1.60E-01
MS_4(823,3)	10.00 ± 0.08	2.50 ± 0.08	2.35E−02 ± 2.35E-03	97.19 ± 1.92	0.9823 ± 0.0042	1.03E + 00 ± 4.41E-01
MS_6(823,3)	10.00 ± 0.08	2.44 ± 0.10	2.55E−02 ± 1.82E-03	94.29 ± 2.13	0.9696 ± 0.0146	2.31E + 00 ± 9.39E-01
MS_8(823,3)	10.00 ± 0.08	2.38 ± 0.10	2.79E−02 ± 2.04E-03	91.27 ± 3.99	0.9594 ± 0.0191	3.47E + 00 ± 1.28E + 00
MS_{10}(823,3)	10.00 ± 0.08	2.39 ± 0.20	2.08E−02 ± 1.77E-04	85.22 ± 3.24	0.9523 ± 0.0112	4.40E + 00 ± 9.22E-01
MS_4(723,3)	10.00 ± 0.08	2.60 ± 0.14	3.77E−02 ± 3.46E-04	90.53 ± 1.24	0.9407 ± 0.0021	4.05E + 00 ± 2.70E-01
MS_4(923,3)	10.00 ± 0.08	2.59 ± 0.13	1.66E−02 ± 2.19E-04	89.88 ± 4.44	0.9741 ± 0.0072	2.00E + 00 ± 1.32E + 00
MS_4(1023,3)	10.00 ± 0.08	2.64 ± 0.15	1.28E−02 ± 8.77E-04	61.57 ± 2.56	0.9350 ± 0.0426	8.24E + 00 ± 2.54E-01
MS_4(1123,3)	10.00 ± 0.08	2.65 ± 0.13	4.50E−03 ± 2.12E-04	52.26 ± 0.46	0.9424 ± 0.0534	2.51E + 00 ± 2.32E + 00
MS_4(823,1)	10.00 ± 0.08	2.65 ± 0.07	2.35E−02 ± 1.17E-03	90.04 ± 1.05	0.9419 ± 0.0126	3.30E + 00 ± 3.01E-01
MS_4(823,6)	10.00 ± 0.08	2.68 ± 0.10	2.59E−02 ± 1.25E-02	82.65 ± 1.28	0.9161 ± 0.0469	5.37E + 00 ± 1.23E + 00
MS_4(823,9)	10.00 ± 0.08	2.68 ± 0.15	3.12E−02 ± 2.11E-02	75.58 ± 2.18	0.9073 ± 0.0425	7.30E + 00 ± 2.25E + 00
MS_4(823,12)	10.00 ± 0.08	2.68 ± 0.11	2.22E−02 ± 1.38E-02	73.14 ± 3.97	0.8763 ± 0.1264	6.90E + 00 ± 3.59E + 00
MK_2(823,3)	6.35 ± 0.19	2.62 ± 0.01	1.40E−02 ± 2.62E-04	95.70 ± 0.08	0.9954 ± 0.0003	3.46E−16 ± 7.59E-18
MK_4(823,3)	6.35 ± 0.19	2.58 ± 0.00	1.29E−02 ± 6.65E-04	83.71 ± 2.23	0.9962 ± 0.0007	2.08E + 00 ± 8.15E-01
MK_8(823,3)	6.35 ± 0.19	2.62 ± 0.01	1.33E−02 ± 7.85E-04	72.22 ± 0.80	0.9827 ± 0.0015	5.73E + 00 ± 5.19E-01
MD_2(823,3)	6.35 ± 0.19	2.60 ± 0.03	1.20E−02 ± 4.03E-04	92.25 ± 1.35	0.9868 ± 0.0123	2.76E−16 ± 1.67E-16
MD_4(823,3)	6.35 ± 0.19	3.11 ± 0.02	1.57E−02 ± 1.28E-03	92.50 ± 0.90	0.9975 ± 0.0014	3.45E−01 ± 4.87E-01
MD_8(823,3)	6.35 ± 0.19	2.74 ± 0.04	1.34E−02 ± 7.21E-04	77.09 ± 3.87	0.9975 ± 0.0036	3.84E + 00 ± 1.04E + 00
MFS_6(823,3)	6.35 ± 0.19	2.61 ± 0.01	2.59E−02 ± 4.10E-04	100.00 ± 0.00	0.9915 ± 0.0018	1.51E−16 ± 9.06E-18
MFS_8(823,3)	6.35 ± 0.19	2.61 ± 0.01	1.82E−02 ± 3.75E-04	97.86 ± 1.07	0.9911 ± 0.0048	3.72E−15 ± 5.13E-15
MFS_{12}(823,3)	6.35 ± 0.19	2.61 ± 0.00	1.76E−02 ± 1.84E-04	98.32 ± 0.52	0.9884 ± 0.0046	1.04E−14 ± 1.95E-15

Note: † All the degradation data were used for fitting.

S3). Moreover, the high alkaline conditions for MS-Oxone systems also produced adverse impacts on IBU removal rate and degradation kinetics (Fig. 4(a) and Table S3). Additionally, MS dosages, Oxone concentrations and solution temperature whether at lower or higher levers were found to cause unfavorable influences on IBU degradation efficiency or kinetics (Table S3).

Given the limitation of the first-order kinetic model, we employed a modified two-parameter pseudo-first order kinetic model [63] (see Equation (b)) to describe Oxone-MnO_x/silica induced IBU degradation process. Overall, compared to the pseudo-first order kinetics, IBU degradation processes can be better fitted by the two-parameter pseudo-first order kinetics. For instance, IBU degradation by Oxone-MS systems in the presence of scavengers like methanol and TBA—which cannot be described by pseudo-first order kinetic model—can be fitted by the two-parameter pseudo-first order kinetics (Tables 3 and S3). Interestingly, in the presence of Cl^- ions at high levels, all IBU degradation data over the whole reaction can be well fitted by the modified model with R^2 of 0.9997; however, fitting those data before the reaction time of 100 min by model (a) resulted in low values of both R^2 and k_{obs} (0.1875 and 0.06788 min^{-1}, respectively), which clearly suggested the failure of describing IBU removal by MS-Oxone. The fast degradation kinetics of IBU by Oxone-MS system at high Cl^- levels is probably due to the formation of chloro-species like Cl_2 or HOCl [64], which can accelerate their reactions with parent IBU or intermediates. In addition, fitting results using two models imply that synthetic conditions of MnO_x-based composites can also influence the reaction kinetics of aqueous IBU by activated Oxone (Tables S2 and 2). For the modified model, the higher values of k_p with lower C_u values represent a fast and relatively complete degradation reaction of parent IBU. However, the sole k_p at a higher value or C_u at a lower value cannot well describe the degradation processes. Hence, it should be noted that, on the whole, the pseudo-first order kinetics can better describe the IBU degradation rate (i.e., the speed of IBU degradation by Oxone-MS systems) (if IBU degradation data were properly handled for fitting), while the two-parameter pseudo-first order kinetics can be used to better fit the whole degradation processes (i.e., all IBU degradation data could be used to fit the kinetic model (b) well, but not for the kinetic model (a)) (refer to Tables 2 and 3, S2 and S3 for details on R^2). In some cases, both models can be employed for describing IBU degradation. However, at current stage, developing universal kinetic models for effectively monitoring/assessing the contaminant degradation by APS-AOPs under complex solution chemistry still remains challenging [26].

3.3. Reaction mechanisms

For aqueous IBU-containing Oxone-MS reaction systems, Oxone decomposition is the first step (see reaction (1)). Upon dissolution of Oxone in DI water, HSO_5^- and $SO_4^{2-}$are formed. Then the HSO_5^- could react with MS via electrostatic interactions, surface adsorption and hydrogen/chemical bonding (see reaction (17)). Subsequently, the redox reactions between Mn-based active substances and HSO_5^- and the formation of free radicals along with IBU degradations are involved.

$$\equiv MnO_x(OH)_y + HSO_5^- \rightarrow \equiv MnO_x(OH)_y\text{–}HOOSO_3^- \quad (17)$$

$$\equiv Mn^{II}O_x(OH)_y\text{–}HOOSO_3^- \rightarrow \equiv Mn^{III}O_x(OH)_{y+1} + SO_4^- \quad (18)$$

$$\equiv Mn^{II}O_x(OH)_y\text{–}HOOSO_3^- \rightarrow \equiv Mn^{III}O_x(OH)_y^+ + SO_4^{2-} + OH \quad (19)$$

Table 3
Fitted data for IBU degradation by aqueous Oxone-MS_4(823,3) system under different conditions using a two-parameter pseudo-first-order kinetics model [ξ].

$pH_{initial}$	pH_{after}	Oxone/mM	MS_4/g/L	Temp./K	Solutes	k_p/min^{-1}	IBU removal/%	R^2	C_u/mM
2.81 ± 0.06	2.32 ± 0.02	6.25	1	293	–	2.13E−02 ± 1.17E-03	98.74 ± 0.15	0.9942 ± 0.0015	2.56E−15 ± 2.83E-15
4.26 ± 0.09	2.40 ± 0.00	6.25	1	293	–	2.03E−02 ± 2.14E-03	98.21 ± 0.14	0.9723 ± 0.0320	2.57E−01 ± 3.64E-01
6.35 ± 0.19	2.42 ± 0.04	6.25	1	293	–	2.38E−02 ± 6.36E-05	97.51 ± 0.00	0.9841 ± 0.0002	8.36E−01 ± 3.02E-02
7.87 ± 0.10	2.41 ± 0.00	6.25	1	293	–	2.22E−02 ± 2.90E-04	98.45 ± 0.11	0.9784 ± 0.0028	4.85E−01 ± 8.57E-04
10.00 ± 0.08	2.50 ± 0.08	6.25	1	293	–	2.35E−02 ± 2.35E-03	97.19 ± 1.92	0.9823 ± 0.0042	1.03E + 00 ± 4.41E-01
11.40 ± 0.05	3.02 ± 0.08	6.25	1	293	–	1.79E−02 ± 8.70E-04	57.75 ± 3.78	0.8596 ± 0.0319	1.12E + 01 ± 1.07E + 00
6.35 ± 0.19	2.47 ± 0.00	6.25	1	293	1 mg/L DHA	1.92E−02 ± 3.61E-03	97.12 ± 0.64	0.9742 ± 0.0018	4.14E−01 ± 5.86E-01
6.35 ± 0.19	2.46 ± 0.03	6.25	1	293	5 mg/L DHA	1.69E−02 ± 1.39E-03	96.89 ± 0.68	0.9789 ± 0.0125	2.09E−01 ± 2.95E-01
6.35 ± 0.19	2.41 ± 0.02	6.25	1	293	10 mg/L DHA	1.45E−02 ± 9.97E-04	94.62 ± 0.18	0.9693 ± 0.0159	1.82E−01 ± 2.57E-01
6.35 ± 0.19	2.40 ± 0.01	6.25	1	293	25 mg/L DHA	1.61E−02 ± 2.45E-03	91.28 ± 0.59	0.9593 ± 0.0120	1.62E + 00 ± 5.99E-01
6.35 ± 0.19	2.33 ± 0.01	6.25	1	293	50 mg/L DHA	2.04E−02 ± 1.22E-03	85.18 ± 2.92	0.9097 ± 0.0146	4.66E + 00 ± 5.23E-01
6.35 ± 0.19	2.48 ± 0.01	6.25	1	293	2 mM Cl^-	2.34E−02 ± 1.33E-03	65.81 ± 0.79	0.9136 ± 0.0038	9.54E + 00 ± 3.16E-01
6.35 ± 0.19	2.62 ± 0.01	6.25	1	293	1 mM HCO_3^-	1.50E−02 ± 2.23E-03	84.48 ± 0.69	0.9628 ± 0.0165	2.94E + 00 ± 6.70E-01
6.35 ± 0.19	2.56 ± 0.02	6.25	1	293	2 mM NO_3^-	1.72E−02 ± 7.57E-04	93.21 ± 1.77	0.9754 ± 0.0054	1.34E + 00 ± 2.52E-01
6.35 ± 0.19	2.56 ± 0.02	6.25	1	293	2 mM SO_4^{2-}	1.66E−02 ± 7.78E-04	92.99 ± 0.86	0.9748 ± 0.0014	1.17E + 00 ± 8.76E-02
6.35 ± 0.19	2.57 ± 0.01	6.25	1	293	0.2 mM PO_4^{3-}	1.61E−02 ± 1.73E-03	89.11 ± 0.70	0.9703 ± 0.0142	2.12E + 00 ± 4.36E-01
6.35 ± 0.19	2.45 ± 0.06	6.25	1	293	20 mM Cl^-	4.69E−01 ± 4.74E-03	100.00 ± 0.00	0.9997 ± 0.0001	1.60E−01 ± 1.56E-02
6.35 ± 0.19	5.90 ± 0.02	6.25	1	293	8 mM HCO_3^-	3.76E−03 ± 2.55E-04	49.92 ± 3.16	0.9845 ± 0.0088	5.36E−13 ± 7.53E-13
6.35 ± 0.19	2.54 ± 0.02	6.25	1	293	10 mM NO_3^-	1.59E−02 ± 7.07E-06	94.42 ± 0.03	0.9771 ± 0.0089	5.81E−01 ± 1.12E-01
6.35 ± 0.19	2.64 ± 0.02	6.25	1	293	10 mM SO_4^{2-}	1.49E−02 ± 1.56E-04	92.27 ± 0.24	0.9707 ± 0.0148	8.34E−01 ± 1.01E-01
6.35 ± 0.19	2.67 ± 0.02	6.25	1	293	2 mM PO_4^{3-}	1.44E−02 ± 1.54E-03	82.19 ± 1.44	0.9764 ± 0.0150	3.30E + 00 ± 1.15E + 00
6.35 ± 0.19	2.65 ± 0.01	6.25	0.5	293	–	1.38E−02 ± 3.96E-04	56.82 ± 2.69	0.9331 ± 0.0022	9.84E + 00 ± 4.79E-01
6.35 ± 0.19	2.64 ± 0.00	6.25	2	293	–	3.54E−02 ± 1.03E-03	91.36 ± 0.26	0.9638 ± 0.0013	3.09E + 00 ± 4.37E-02
6.35 ± 0.19	2.91 ± 0.01	3.125	1	293	–	2.78E−02 ± 5.83E-03	46.23 ± 2.04	0.8871 ± 0.0281	1.41E + 01 ± 6.79E-01
6.35 ± 0.19	2.42 ± 0.01	12.5	1	293	–	2.20E−02 ± 3.32E-04	96.23 ± 0.90	0.9614 ± 0.0005	1.54E + 00 ± 2.45E-01
6.35 ± 0.19	2.56 ± 0.06	6.25	1	293	38.597 mM M*	3.75E−02 ± 1.68E-02	36.92 ± 2.35	0.8637 ± 0.0229	1.63E + 01 ± 1.77E-01
6.35 ± 0.19	2.56 ± 0.01	6.25	1	293	153.496 mM M*	8.09E−02 ± 4.44E-02	19.32 ± 2.67	0.9159 ± 0.1137	2.00E + 01 ± 4.29E-03
6.35 ± 0.19	2.53 ± 0.07	6.25	1	293	610.194 mM M*	1.27E−01 ± 6.70E-03	17.68 ± 1.81	0.9141 ± 0.0613	2.04E + 01 ± 2.31E-01
6.35 ± 0.19	2.55 ± 0.04	6.25	1	293	38.597 mM T†	2.01E−02 ± 5.47E-03	71.97 ± 0.26	0.9371 ± 0.0154	7.14E + 00 ± 7.57E-01
6.35 ± 0.19	2.60 ± 0.05	6.25	1	293	153.496 mM T†	2.40E−02 ± 2.02E-03	52.60 ± 1.96	0.9183 ± 0.0183	1.23E + 01 ± 5.40E-01
6.35 ± 0.19	2.59 ± 0.04	6.25	1	293	610.194 mM T†	4.36E−02 ± 2.30E-03	24.43 ± 1.82	0.9108 ± 0.0447	1.87E + 01 ± 2.84E-01
6.35 ± 0.19	2.58 ± 0.00	6.25	1	283	–	1.45E−02 ± 6.15E-04	54.02 ± 2.45	0.9542 ± 0.0012	1.09E + 01 ± 2.19E-01
6.35 ± 0.19	2.66 ± 0.00	6.25	1	313	–	2.57E−02 ± 6.22E-04	100.00 ± 0.00	0.9958 ± 0.0013	9.55E−17 ± 3.33E-17

Notes: M* and T† stand for methanol and TBA, respectively; [ξ] All the degradation data were used for fitting.

$$\equiv Mn^{IV}O_x(OH)_y\text{–}HOOSO_3^- \rightarrow \equiv Mn^{III}O_{x+y}H_{y+1} + SO_5^{\bullet -} \quad (20)$$

$$\equiv Mn^{III}O_{x+y}H_{y+1} + HSO_5^- \rightarrow Mn^{III}O_{x+y}H_{y+1}\text{–}HOOSO_3^- \quad (21)$$

$$\equiv Mn^{III}O_{x+y}H_{y+1}\text{–}HOOSO_3^- \rightarrow \equiv Mn^{IV}O_{x+y+1}H_{y+2} + SO_4^{\bullet -} \quad (22)$$

$$SO_4^{\bullet -} + H_2O \rightarrow OH + SO_4^{2-} + H^+ \quad (23)$$

$$OH + SO_4^{\bullet -} + IBU + H_2O \rightarrow \text{products} + SO_4^{2-} + H^+ \quad (24)$$

3.3.1. Interactions of aqueous oxone-MS systems

XPS analysis (see Table 4) clearly indicates the presence of multivalent MnO_x species within MS_4(823,3), while in-situ ATR-IR characterizations definitely imply the existence of surface hydroxyl groups on MS_4(823,3) (see Fig. 5(a)). These distinct features of MS_4(823,3) composites are conducive to the multiple reactions between HSO_5^- and the $\equiv MnO_x(OH)_y$ of MS_4(823,3). For instance, $\equiv Mn^{III}O_x(OH)_y$ can react with HSO_5^- to form $SO_4^{\bullet -}/SO_5^{\bullet -}$ by disproportionation reaction [14], while $\equiv Mn^{II}O_x(OH)_y$ and $\equiv Mn^{IV}O_x(OH)_y$ may induce HSO_5^- to produce $SO_4^{\bullet -}$ and $SO_5^{\bullet -}$ via oxidation and reduction processes, respectively [31,50]. The detected changes in valence state of $\equiv MnO_x(OH)_y$ before and after reaction (cf. Table 3) confirmed the redox processes of Mn-based species in the surface activation of Oxone.

In the light of previous studies [27,28,56,65,66], peaks at around 1240 cm^{-1} and 1104 cm^{-1} in ATR-IR for Oxone sample (Fig. 5(a)) can be ascribed to the S—O stretching vibrations of HSO_5^- and SO_4^{2-}decomposed from Oxone in aqueous phase. Two distinct peaks appeared in in-situ Raman spectra at around 982 cm^{-1} and 1062 cm^{-1} and a broad weak peak at about 880 cm^{-1} (Fig. 5(b)) further confirm the presence of S—O stretching bonds of HSO_5^- and SO_4^{2-} [28]. A slight red shift (by ~10 cm^{-1}) of the S—O band from about 1104 cm^{-1} to 1094 cm^{-1} occurred after MS_4(823,3) was added. This shift in the S—O band of HSO_5^- implies that (1) some complex compounds (like $\equiv MnO_x(OH)_y\text{–}(HO)OSO_3^-$) formed on MS_4(823,3) surface (cf. reaction (17)), and (2) at the same time, Oxone decomposition subsequently happened along with the formation of intermediates (such as peroxo active species) on the surface. The apparent shift of S—O band that would occur is largely dependent on the types of persulfate-activator systems [27,28,66]. The red-shift of S—O band indicates that, in general, the electron density of S—O in HSO_5^- decreased by electron–donating/withdrawing reactions of $\equiv MnO_x(OH)_y$ substances and HSO_5^-. On one hand, the electron-donating process from surface $\equiv Mn^{II}O_x(OH)_y$ to the terminal —OH group of HSO_5^- and/or the potential formation of hydrogen bonds between —OH of HSO_5^- and —OH of $\equiv Mn^{II}O_x(OH)_y$, to some extent, can inhibit the electron-withdrawing ability of —OH group in HSO_5^- from its neighboring S—O, thus causing S—O bonds to be stronger and leading to the blue shift of S—O bonds; on the other hand, the —OH group of HSO_5^- bonded to MS_4(823,3) surface by strong electron attraction of $\equiv Mn^{IV}O_x(OH)_y$ could draw more electron density from S—O bonds, which makes S—O stretching bonds become weaker, thereby causing a red shift. Note that the reactions of terminal —OH group of HSO_5^- with $\equiv Mn^{III}O_x(OH)_y$ can lead to blue and/or red shifts via their electron–donating and/or –withdrawing processes. However, the detected red-shift of HSO_5^- stretching bond could be ascribed to a trade-off of the aforementioned contradictory reactions between $\equiv MnO_x(OH)_y$ and HSO_5^-. Interestingly, a red shift by 41 cm^{-1} of S—O bonds from 1121 cm^{-1} to 1080 cm^{-1} was also observed in ATR-IR spectra for dry Oxone-MS_4(823,3) and Oxone samples (Fig. S16), again confirming the findings above. This difference in red shift of S—O bonds lies in the difference of sample properties by two preparing methods. In addition, when H_2O spectrum as background subtracted, remarkable IR spectra appearing at 3307–3376 cm^{-1} were also detected for all samples, indicating the

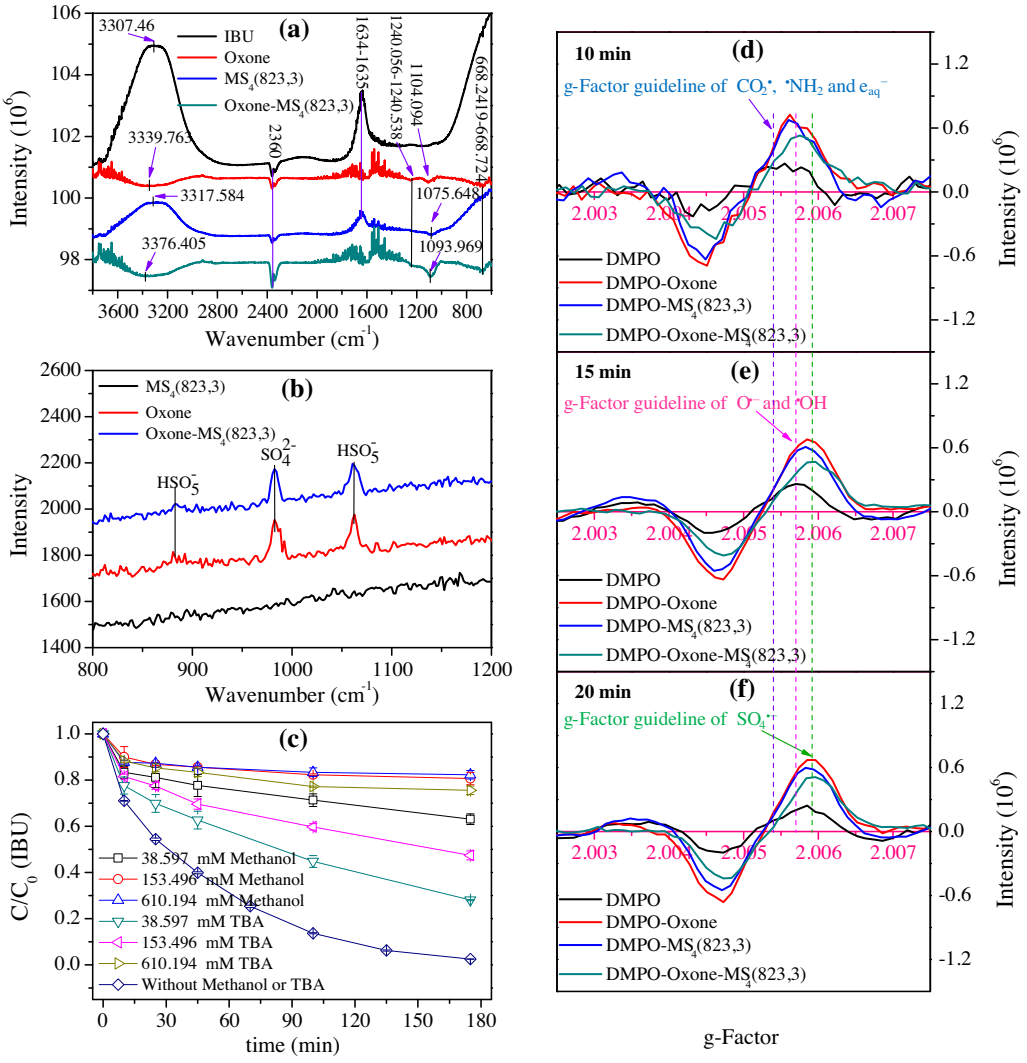

Fig. 5. (a) ATR-IR spectra for IBU, Oxone, $MS_4(823,3)$, and Oxone–$MS_4(823,3)$ in IBU solutions (without pH adjustment). The water spectrum has been subtracted from all above spectra. (b) Raman spectra recorded from the cases of $MS_4(823,3)$, Oxone and $MS_4(823,3)$ and Oxone in IBU solutions (without pH adjustment). Samples were withdrawn at reaction time of 90 min, and the record time and record depth for all testing samples were 60 s and 300 nm, respectively. (c) Effects of alcohols on IBU removal by MS-Oxone systems. (d–f) Changes of EPR signals (i.e., g-Factor vs Intensity) detected in different systems at different reaction time. Reaction conditions for (a) and (b): $[MS_4(823,3)]_0 = 4$ g/L, $[IBU]_0 = 24.24$ μM, $[Oxone]_0 = 25$ mM. Conditions for (c): $[IBU]_0 = 24.24$ μM, $[Oxone]_0 = 6.25$ mM, $[MS_4(823,3)]_0 = 1.0$ g/L, volume of 80 mL, reaction temperature of 298 K, reaction time of 175 min and $pH_0 = 6.35 \pm 0.2$. Conditions for (d–f): $[Oxone]_0 = 5$ mM, $[MS_4(823,3)]_0 = 0.5$ g/L, $pH_0 = 6.35 \pm 0.2$, $[DMPO]_0 = 0.2$ M.

Table 4
XPS analysis of surface Mn element of fresh and aged $MS_4(823,3)$.

Samples	Valence state of Mn (%)			Average valence of Mn
	IV	III	II	
$MS_4(823,3)$	45.79	33.29	20.92	3.2487
Aged $MS_4(823,3)$	31.12	32.09	36.79	2.9433

presence of considerable surface —OH groups/water moieties likely due to strong adsorption of water molecules and —OH groups from HSO_5^- decomposition and H_2O dissociation. For the case of Oxone-$MS_4(823,3)$, the peaks for —OH groups blue-shifted by 59 cm^{-1} and 37 cm^{-1} compared to those of $MS_4(823,3)$ and Oxone, respectively. The results indicate that (1) the —OH in HSO_5^- had bonded to $MS_4(823,3)$ surface, and (2) the electron-donating capability of $\equiv MnO_x(OH)_y$ had increased, possibly due to the decreased transient valence of Mn (see Table 4). The two processes can result in the increased electron density of the —OH bonds in HSO_5^- and $MS_4(823,3)$ surface, which in turn leads to the occurrence of blue-shift of —OH groups. The clear peak at ~3307 cm^{-1} in ATR-IR for IBU indicates its strong adsorption toward H_2O molecules probably through the formation of hydrogen bonds with —COOH groups (evidenced by apparent peak at around 1634 cm^{-1} for IBU in Fig. 5(a)). The peak at around 1635 cm^{-1} for $MS_4(823,3)$ sample may be due to the residual —COO— groups derived from MnO_x precursors. The peaks at around 668 cm^{-1} in Fig. 5(a) and at 534–668 cm^{-1} in Fig. S16 also attest the interactions of Oxone-$MS_4(823,3)$ system [65,67].

3.3.2. RORs in aqueous oxone-MS systems

For aqueous Oxone-MS systems, the electron transfer process between $\equiv MnO_x(OH)_y$ and HSO_5^- is of great

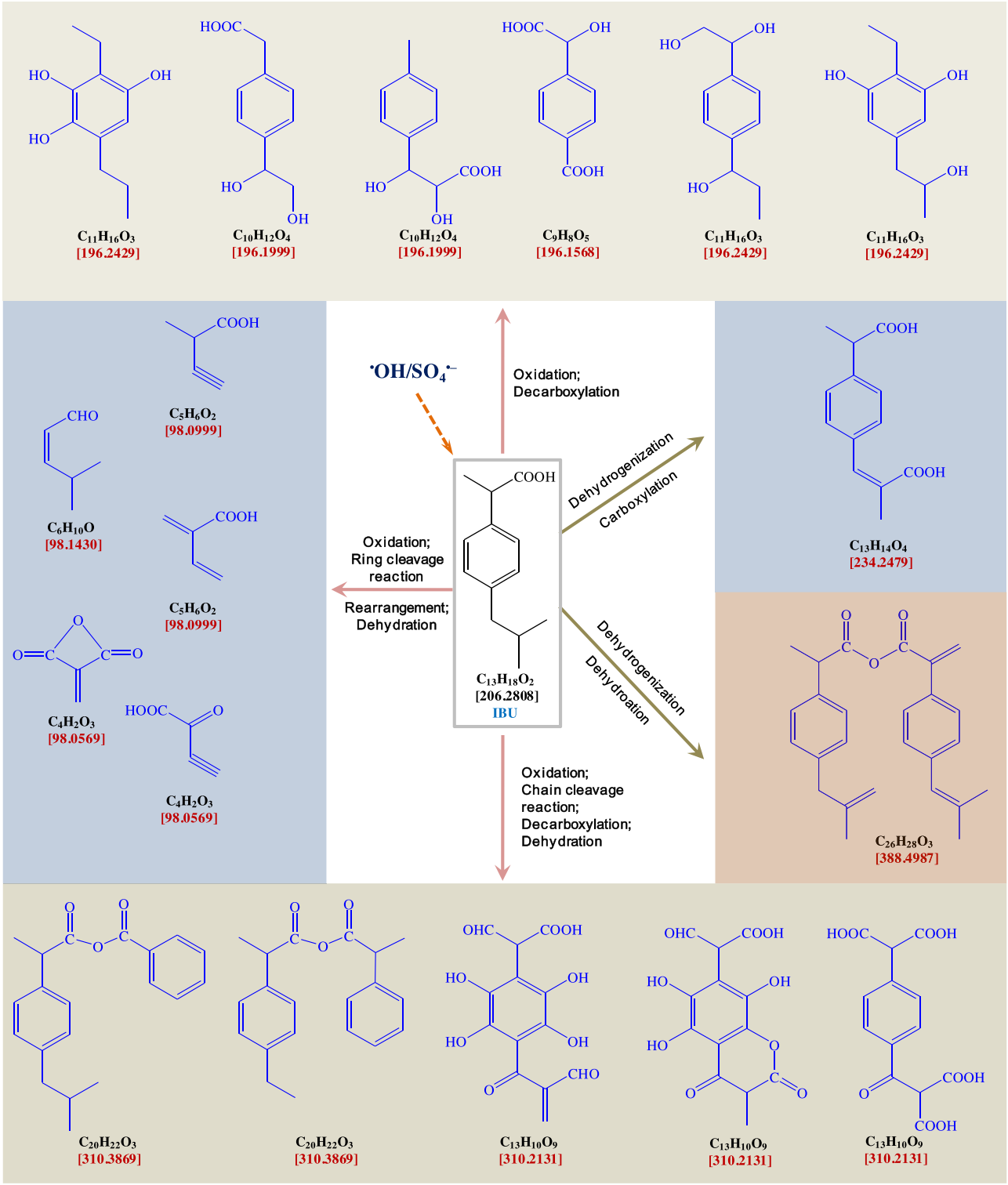

Fig. 6. Schematic demonstration of IBU degradation by Oxone-MS_4(823,3) system (see Figs. S18–S24 for details).

Table 5
Inhibition of different alcohols to IBU removal (%) by aqueous Oxone-MS_4(823,3) system.

Concentrations of alcohols (mM)	Methanol	TBA	Inhibition (%)	
			Methanol	TBA
0	97.51 ± 3.13E-3	97.51 ± 3.13E-3	0	0
38.60	36.92 ± 2.35E0	71.97 ± 2.62E-1	62.14	26.19
153.50	19.32 ± 2.67E0	52.60 ± 1.96E0	80.19	46.06
610.19	17.68 ± 1.81E0	24.43 ± 1.82E0	81.87	74.95

importance for generations of active radicals in aqueous phase. *tert*-butyl alcohol (TBA) without an alpha hydrogen was reported to effectively inhibit the reaction activities of •OH (i.e., •OH scavenger ($K_{TBA-OH} = 6.0 \times 10^8\ M^{-1}\ s^{-1}$)) but not for $SO_4^{\bullet-}$($K_{TBA-SO} = 4.0 \times 10^5\ M^{-1}\ s^{-1}$) in aquatic phase, while methanol with an α hydrogen could react with both $SO_4^{\bullet-}$and •OH (i.e., $SO_4^{\bullet-}$/•OH scavengers ($K_{M-SO} = 9.7 \times 10^8\ M^{-1}\ s^{-1}$, $K_{M-OH} = 3.2 \times 10^6\ M^{-1}\ s^{-1}$)) [68,69]. The molar concentrations of alcohols used in the current work are $(1.59–25.17) \times 10^3$ times higher than that of IBU in MS-Oxone reaction systems. If IBU were mainly oxidized by $SO_4^{\bullet-}$in aqueous solution, the addition of TBA would not lead to great decrease in IBU degradation. Nevertheless, the removal rates of parent IBU decreased progressively with the prolonged reaction time and increased TBA (Fig. 5(c)). The decreased IBU removal due to the TBA introduction indicates that •OH was formed in the reaction system and also contributed to IBU degradation. The correspondingly decreased IBU removal and the difference of decreased IBU removal caused by TBA and methanol additions at the similar concentrations (Fig. 5(c) and Table 5) imply that both $SO_4^{\bullet-}$ and •OH are produced in the reaction systems, which thus favored IBU degradation.

5,5-dimethyl-1-pyrroline N-oxide (DMPO) as a spin-trapping agent has been used for capturing radicals in aqueous solutions. Prominent EPR signals were observed in the current study (Figs. 5 (d–f) and S17), indicating the formation of RORs in aquatic systems. The relatively longer radicals are also recently reported for organic degradation during persulfate activation by heterogeneous processes [70]. As shown in Fig. 5(d–f), similar trends for g-Factor changes (i.e., all g-Factors increased with prolonged time in a range from 2.00555 to 2.00596) were observed for all cases, which suggested the formation of some oxygen-centered radicals and their evolution. Previous studies indicated that g-Factors having values of 2.0054 ± 0.0001, 2.0057 ± 0.0001 and 2.0059 ± 0.0001 stand for the presence of e_{aq}^-, •OH/$O^{\bullet-}$ and $SO_4^{\bullet-}$, respectively [71]. Weak EPR signals detected for DMPO in water might be ascribed to the nonradical nucleophilic reaction of DMPO with water [72], while relative high EPR signals for DMPO in aquatic Oxone or MS_4(823,3) (Fig. S17) solutions were attributed to the nitroxide radicals of 5,5-dimethylpyrroline-2-oxyl-(1) (DMPOX) resulted from direct oxidation by single electron substances (but not derived from spin-trapping of DMPO-•OH) [27,50,71]. For aquatic Oxone-MS_4(823,3) system, g-Factor increased from 2.00575 to 2.00596 with time from 10 min to 20 min, revealing the formation of DMPO−SO_4^- and DMPO−OH radical adducts [50,71], which suggests that •OH and $SO_4^{\bullet-}$ are major RORs in Oxone-MS_4(823,3) system [73] and confirms the above scavenging experiments. Note that, regardless of the fact that $SO_4^{\bullet-}$ can be partially converted into •OH (see reaction (23)), •OH and $SO_4^{\bullet-}$ radicals can form simultaneously by electron transport processes between ≡$MnO_x(OH)_y$ substances and HSO_5^- in aquatic Oxone-MS_4(823,3) system (see reactions (18) and (19)), evidenced by the mentioned XPS analysis and EPR characterization. Generally, various characterizations and quenching experiments suggest that multiple oxidation states of MnO_x species in MS composite play multiple and vital roles in ROR formations (see reactions (17)–(23)), and that the interactions and ROR formations for aqueous Oxone-MS_4(823,3) system are quite complex.

3.3.3. By-products in aqueous oxone-MS systems

LC–MS/MS analysis (cf. Figs. S18 and S19) showed various by-products from IBU degradation. The possible by-products and tentative reaction pathways are depicted in Figs. 6 and S20–S24. It's clear that the degradation/transformation processes of IBU mainly involve hydroxylation, carboxylation/decarboxylation, dehydrogenization and ring/chain cleavage, caused by the oxidation of •OH and $SO_4^{\bullet-}$. When •OH and $SO_4^{\bullet-}$ induced the hydroxylation, carboxylation and/or decarboxylation of IBU, some hydroxylated and/or carboxylated byproducts with *m*/*z* of 194.5 or 194.9 were formed (Figs. 6 and S21), while if IBU was strongly attacked by radicals, ring/chain cleavage reactions would occurred with some other intermediate products formed with *m*/*z* of 96.9/96.5 or of 308.4/308.9 (Figs. 6, S20 and S23(C–E)). Some other oxidation and dehydrogenization processes also resulted in formation of byproducts with *m*/*z* of 232.6 and 308.4/308.9 (see details in Figs. 6, S22 and S23(A,B)). The intramolecular and intermolecular dehydration reactions of aromatic intermediates were also observed (Figs. 6, S23(C–E) and S24), which led to the formation of final byproducts (*m*/*z*, 308.4/308.9 and 387.5). Unexpectedly, the byproducts of IBU degradation detected in the current work were different from the previous reports by other AOPs like sonophotocatalysis, electro-peroxone and photocatalytic treatment [74–76]. The differences in distribution of byproducts might be due to the different RORs in the oxidation systems. The formation of various byproducts for IBU degradation by Oxone-MS_4(823,3) system, on one hand, indicated the non-selectivity of •OH and $SO_4^{\bullet-}$ for organic degradation, but on the other hand, suggested the limited oxidation ability of Oxone-MS_4(823,3) system for IBU degradation, evidenced by the low TOC removal of IBU (<20%) (much lower than that of butyl baraben by Oxone-MS system in our previous wok [18]). The possible explanation might be the anti-degradation properties of IBU due to its electron-withdrawing functional group (−COOH) [26] and the higher apparent activation energy (E_a = 44.4 kJ/mol, calculated by Arrhenius equation using k_{obs} values under different solution temperature (Table S3)) for reactions between IBU and Oxone-MS_4(823,3) system [14,16,50]. Although the byproducts of IBU degradation were preliminarily detected and analyzed, yet the accurate identification of the byproducts and their eco-toxicity warrant further studies.

4. Conclusions

Synthesis conditions of MnO_x/silica composites generated notably different effects on catalytic Oxone efficacy for IBU removal, and the water chemistry constituents, like humic acid, Cl^-, NO_3^-, HCO_3^-, SO_4^{2-} and PO_4^{3-} also exerted ingredient and concentration-dependent influences on IBU removal by Oxone-MS system. IBU reaction kinetics by Oxone-MnO_x/silica systems was largely dependent on the extents of the interferences of synthetic conditions and water chemistry components. The mechanisms for IBU degradation involved the surface electron transfer between ≡$MnO_x(OH)_y$ species of MS and HSO_5^- of Oxone and the formation of RORs. Oxidation products of IBU were identified by LC–MS/MS, and hydroxylation, carboxylation/decarboxylation, dehydrogenization, chain/ring cleavage reaction and dehydration were proposed as the main processes contributing to IBU degradation. This work will advance our understanding on the catalytic Oxone efficacies of MnO_x/silica systems towards pollutant degradation, thus enabling us to manipulate functional catalysts for specific environmental applications.

Acknowledgments

The authors greatly acknowledge Ms. Dan-Dan Zhang from the IUE, CAS and Ms. La-Jia Yu in Xiamen University, China, respectively, for their help in Raman/ATR-IR and EPR measurements. This research was partially supported by National Natural Science Foundation of China (Grant Nos. 51278481 and 51478449) and International Science & Technology Cooperation Program of China (2011DFB91710).

Appendix A. Supplementary data

Supplementary data associated with this article can be found, in the online version, at http://dx.doi.org/10.1016/j.apcatb.2016.12.046.

References

[1] P. Hu, M. Long, Appl. Catal. B: Environ. 181 (2016) 103–117.
[2] G.P. Anipsitakis, D.D. Dionysiou, Environ. Sci. Technol. 37 (2003) 4790–4797.
[3] W. Oh, Z. Dong, T. Lim, Appl. Catal. B: Environ. 194 (2016) 169–201.
[4] Y. Gao, S. Li, Y. Li, L. Yao, H. Zhang, Appl. Catal. B: Environ. 202 (2017) 165–174.
[5] Y. Gao, Z. Zhang, S. Li, J. Liu, L. Yao, Y. Li, H. Zhang, Appl. Catal. B: Environ. 185 (2016) 22–30.
[6] X. Duan, C. Su, L. Zhou, H. Sun, A. Suvorova, T. Odedairo, Z. Zhu, Z. Shao, S. Wang, Appl. Catal. B: Environ. 194 (2016) 7–15.
[7] Y. Wang, Z. Ao, H. Sun, X. Duan, S. Wang, Appl. Catal. B: Environ. 198 (2016) 295–302.
[8] R.R. Solís, F.J. Rivas, O. Gimeno, Appl. Catal. B: Environ. 200 (2017) 83–92.
[9] J. Li, Q. Liu, Q.Q. Ji, B. Lai, Appl. Catal. B: Environ. 200 (2017) 633–646.
[10] Z. Xu, C. Shan, B. Xie, Y. Liu, B. Pan, Appl. Catal. B: Environ. 200 (2017) 439–447.
[11] G. Fang, W. Wu, C. Liu, D.D. Dionysiou, Y. Deng, D. Zhou, Appl. Catal. B: Environ. 202 (2017) 1–11.
[12] H. Liu, T.A. Bruton, W. Li, J.V. Buren, C. Prasse, F.M. Doyle, D.L. Sedlak, Environ. Sci. Technol. 50 (2016) 890–898.
[13] X. Duan, Z. Ao, L. Zhou, H. Sun, G. Wang, S. Wang, Appl. Catal. B: Environ. 188 (2016) 98–105.
[14] E. Saputra, S. Muhammad, H. Sun, H. Ang, M.O. Tadé, S. Wang, Appl. Catal. B: Environ. 142–143 (2013) 729–735.
[15] S. Indrawirawan, H. Sun, X. Duan, S. Wang, Appl. Catal. B: Environ. 179 (2015) 352–362.
[16] E. Saputra, S. Muhammad, H. Sun, H. Ang, M.O. Tadé, S. Wang, Appl. Catal. B: Environ. 154–155 (2014) 246–251.
[17] Y. Ren, L. Lin, J. Ma, J. Yang, J. Feng, Z. Fan, Appl. Catal. B: Environ. 165 (2015) 572–578.
[18] J.E. Yang, H. Lan, X. Lin, B. Yuan, M. Fu, Chem. Eng. J. 289 (2016) 296–305.
[19] O.S. Furman, A.L. Teel, R.J. Watts, Environ. Sci. Technol. 44 (2010) 6423–6428.
[20] Y. Guan, J. Ma, X. Li, J. Fang, L. Chen, Environ. Sci. Technol. 45 (2011) 9308–9314.
[21] Z. Wang, R. Yuan, Y. Guo, L. Xu, J. Liu, J. Hazard. Mater. 190 (2011) 1083–1087.
[22] T. Zhou, X. Zou, J. Mao, X. Wu, Appl. Catal. B: Environ. 185 (2016) 31–41.
[23] G. Fang, D.D. Dionysiou, Y. Wang, S.R. Al-Abed, D. Zhou, J. Hazard. Mater. 227–228 (2012) 394–401.
[24] C. Liang, Z. Wang, N. Mohanty, Sci. Total Environ. 370 (2006) 271–277.
[25] J. Sharma, I.M. Mishra, D.D. Dionysiou, V. Kumar, Chem. Eng. J. 276 (2015) 193–204.
[26] Y. Qian, X. Guo, Y. Zhang, Y. Peng, P. Sun, C. Huang, J. Niu, X. Zhou, J.C. Crittenden, Environ. Sci. Technol. 50 (2016) 772–781.
[27] Y. Feng, D. Wu, Y. Deng, T. Zhang, K. Shih, Environ. Sci. Technol. 50 (2016) 3119–3127.
[28] T. Zhang, H. Zhu, J. Croué, Environ. Sci. Technol. 47 (2013) 2784–2791.
[29] Y. Ding, L. Zhu, N. Wang, H. Tang, Appl. Catal. B: Environ. 129 (2013) 153–162.
[30] L. Hu, X. Yang, S. Dang, Appl. Catal. B: Environ. 102 (2011) 19–26.
[31] S. Luo, L. Duan, B. Sun, M. Wei, X. Li, A. Xu, Appl. Catal. B: Environ. 164 (2015) 92–99.
[32] X. Duan, H. Sun, Y. Wang, J. Kang, S. Wang, ACS Catal. 5 (2015) 553–559.
[33] K. Zhang, X. Han, Z. Hu, X. Zhang, Z. Tao, J. Chen, Chem. Soc. Rev. 44 (2015) 699–728.
[34] P. Sudarsanam, B. Hillary, M.H. Amin, S.B.A. Hamid, S.K. Bhargava, Appl. Catal. B: Environ. 185 (2016) 213–224.
[35] N.M. Vieno, T. Tuhkanen, L. Kronberg, Environ. Sci. Technol. 39 (2005) 8220–8226.
[36] H. Buser, T. Poiger, M.D. Müller, Environ. Sci. Technol. 33 (1999) 2529–2535.
[37] F. Méndez-Arriaga, S. Esplugas, J. Giménez, Water Res. 44 (2010) 589–595.
[38] D. Xia, I.M.C. Lo, Water Res. 100 (2016) 393–404.
[39] F. Méndez-Arriaga, S. Esplugas, J. Giménez, Water Res. 42 (2008) 585–594.
[40] Y. Xiang, J. Fang, C. Shang, Water Res. 90 (2016) 301–308.
[41] A. Kaur, A. Umar, S.K. Kansal, Applied Catalysis, A: Gen. 510 (2016) 134–155.
[42] J. Bing, C. Hu, Y. Nie, M. Yang, J. Qu, Environ. Sci. Technol. 49 (2015) 1690–1697.
[43] D.Y. Zhao, J.L. Feng, Q.S. Huo, N. Melosh, G.H. Fredrickson, B.F. Chmelka, G.D. Stucky, Science 279 (1998) 548–552.
[44] C. Reed, Y. Lee, S.T. Oyama, J. Phys. Chem. B 110 (2006) 4207–4216.
[45] S. Xing, C. Hu, J. Qu, H. He, M. Yang, Environ. Sci. Technol. 42 (2008) 3363–3368.
[46] L. Yang, C. Hu, Y. Nie, J. Qu, Environ. Sci. Technol. 43 (2009) 2525–2529.
[47] E. Saputra, S. Muhammad, H. Sun, H.M. Ang, M.O. Tadé, S. Wang, Environ. Sci. Technol. 47 (2013) 5882–5887.
[48] A.L. Pham, C. Lee, F.M. Doyle, D.L. Sedlak, Environ. Sci. Technol. 43 (2009) 8930–8935.
[49] J. Bing, C. Hu, Y. Nie, M. Yang, J. Qu, Environ. Sci. Technol. 49 (2015) 1690–1697.
[50] Y. Wang, H. Sun, H.M. Ang, M.O. Tadé, S. Wang, Appl. Catal. B: Environ. 164 (2015) 159–167.
[51] F. Wang, H. Dai, J. Deng, G. Bai, K. Ji, Y. Liu, Environ. Sci. Technol. 46 (2012) 4034–4041.
[52] C. Ràfols, M. Rosés, E. Bosch, Anal. Chim. Acta 338 (1997) 127–134.
[53] Y. Yang, J. Jiang, X. Lu, J. Ma, Y. Liu, Environ. Sci. Technol. 49 (2015) 7330–7339.
[54] Z. Wang, R. Yuan, Y. Guo, L. Xu, J. Liu, J. Hazard. Mater. 190 (2011) 1083–1087.
[55] R. Yuan, S.N. Ramjaun, Z. Wang, J. Liu, J. Hazard. Mater. 196 (2011) 173–179.
[56] Y. Lei, C. Chen, Y. Tu, Y. Huang, H. Zhang, Environ. Sci. Technol. 49 (2015) 6838–6845.
[57] L.R. Bennedsen, J. Muff, E.G.S. Gaard, Chemosphere 86 (2012) 1092–1097.
[58] X. Wu, X. Gu, S. Lu, Z. Qiu, Q. Sui, X. Zang, Z. Miao, M. Xu, Sep. Purif. Technol. 147 (2015) 186–193.
[59] P. Maruthamuthu, P. Neta, J. Phys. Chem. 82 (1978) 710–713.
[60] P. Maruthamuthu, P. Neta, J. Phys. Chem. 81 (1977) 1622–1625.
[61] C. Tan, N. Gao, Y. Deng, J. Deng, S. Zhou, J. Li, X. Xin, J. Hazard. Mater. 276 (2014) 452–460.
[62] L.W. Matzek, K.E. Carter, Chemosphere 151 (2016) 178–188.
[63] H. Shu, M. Chang, H. Yu, W. Chen, J. Colloid Interf. Sci. 314 (2007) 89–97.
[64] H.V. Lutze, N. Kerlin, T.C. Schmidt, Water Res. 72 (2015) 349–360.
[65] J. Gonzalez, M. Torrent-Sucarrat, J.M. Anglada, Phys. Chem. Chem. Phys. 12 (2010) 2116–2125.
[66] T. Zhang, Y. Chen, Y. Wang, J. Le Roux, Y. Yang, J. Croué, Environ. Sci. Technol. 48 (2014) 5868–5875.
[67] Z. Chen, Z. Jiao, D. Pan, Z. Li, M. Wu, C. Shek, C.M.L. Wu, J.K.L. Lai, Chem. Rev. 112 (2012) 3833–3855.
[68] P. Neta, R.E. Huie, A.B. Ross, J. Phys. Chem. Ref. Data 17 (1988) 1027–1284.
[69] G.V. Buxton, C.L. Greenstock, W.P. Helman, A.B. Ross, J. Phys. Chem. Ref. Data 17 (1988) 513–886.
[70] G. Fang, C. Liu, J. Gao, D.D. Dionysiou, D. Zhou, Environ. Sci. Technol. 49 (2015) 5645–5653.
[71] Y. Kirino, T. Ohkuma, T. Kwan, Chem. Pharm. Bull. 29 (1981) 29–34.
[72] W. Chamulitrat, H. Iwahashi, D.J. Kelman, R.P. Mason, Arch. Biochem. Biophys. 296 (1992) 645–649.
[73] G. Fang, D.D. Dionysiou, S.R. Al-Abed, D. Zhou, Appl. Catal. B: Environ. 129 (2013) 325–332.
[74] J. Madhavan, F. Grieser, M. Ashokkumar, J. Hazard. Mater. 178 (2010) 202–208.
[75] X. Li, Y. Wang, S. Yuan, Z. Li, B. Wang, J. Huang, S. Deng, G. Yu, Water Res. 63 (2014) 81–93.
[76] F. Méndez-Arriaga, S. Esplugas, J. Giménez, Water Res. 42 (2008) 585–594.